 FDMP, vol.6, no.1, pp.13-40, 2010

Rayleigh-Marangoni Instability of Binary Fluids with Small Lewis Number and Nano-Fluids in the Presence of the Soret Effect

A. Podolny[1,2], A. Nepomnyashchy[3] and A. Oron[4]

Abstract: A general model for two-component transport phenomena applicable for both nanofluids and binary solutions is formulated. We investigate a combined long-wave Marangoni and Rayleigh instability of a quiescent state of a binary (nano-) liquid layer with a non-deformable free surface. The layer is heated from below or from above. The concentration gradient is induced due to the Soret effect. A typical behavior of monotonic and oscillatory instability boundaries is examined in the limit of asymptotically small Lewis numbers and poorly conducting boundaries in the two important long-wave domains $k \sim Bi^{1/2}$ and $k \sim Bi^{1/4}$.

Keywords: nanofluids, Marangoni convection, Rayleigh convection, Soret effect

1 Introduction

Investigation of the combined buoyancy-driven (Rayleigh) and surface-tension-driven (Marangoni) convection in binary fluids was started several decades ago [Nield (1967); Castillo and Velarde (1978)]. A special attention was paid to the instability of a quiescent liquid layer subject to an imposed vertical temperature gradient, when the concentration gradient is produced by the Soret effect (see [Cross and Hohenberg (1993); Oron and Nepomnyashchy (2004)] and the references therein). An essential progress in understanding the instability phenomena was achieved in the case of nearly insulated boundaries, i.e., small Biot number Bi (see [Podolny, Nepomnyashchy, and Oron (2008)]), where a longwave instability was considered.

[1] Department of Mathematics, Technion-Israel Institute of Technology, Haifa 32000, Israel
[2] Present address (address for correspondence): Engineering Sciences and Applied Mathematics, Northwestern University, Evanston, IL 60208, USA
[3] Department of Mathematics and Minerva Center for Nonlinear Physics of Complex Systems, Technion-Israel Institute of Technology, Haifa 32000, Israel
[4] Department of Mechanical Engineering, Technion- Israel Institute of Technology, Haifa 32000, Israel

However, a binary fluid has one more natural small parameter that is the Lewis number L, i.e., the ratio of the characteristic heat conduction time and the diffusion time. This parameter is especially small for a new class of fluids, nanofluids, where the role of solute molecules is played by nanoparticles in the size range of about 10 to 50 nm. From the point of view of dynamics and heat/mass transfer, a typical nanofluid behaves as a Newtonian binary fluid with an extremely small Lewis number ($L \leq 10^{-4}$) and high Soret coefficient ($\sim 10 - 10^2$) [Shliomis and Souhar (2000); Mazzoni, Cerbino, Brogioli, Vailati, and Giglio (2004); Kim, Hong, and Choi (2006)]. There is a significant number of publications on the buoyancy convection in nanofluids [Shliomis and Souhar (2000); Mazzoni, Cerbino, Brogioli, Vailati, and Giglio (2004); Kim, Hong, and Choi (2006); Xuan and Li (2000); Xuan and Roetzel (2000); Khanafer, Vafai, and Lightstone (2003); Kim, Kang, and Choi (2004); Savino and Paterna (2008)], including binary nanofluids [Ryskin, Muller, and Pleiner (2003); Kim, Kang, and Choi (2005); Kim, Jung, and Kang (2007); Kim, Kang, and Choi (2007)]. The Marangoni convection in nanofluids is still scarcely investigated, though an essential influence of nanoparticles on surface tension was revealed in some experiments [Xue, Fan, Hu, Hong, and Cen (2006); Dong and Johnson (2003b); Dong and Johnson (2003a); Ravera, Ferrari, Liggieri, Loglio, Santini, and Zanobini (2008)]. The latter phenomenon can be significant for applications of nanofluids in boiling devices [Xue, Fan, Hu, Hong, and Cen (2006)], including those used in microgravity conditions. Nanofluids with a free surface are used in heat pipes, therefore the problem of interfacial convection in non-isothermal nanofluids is of a great practical importance.

The previous investigation of the longwave Rayleigh-Marangoni convection [Podolny, Nepomnyashchy, and Oron (2008)] was carried out under the assumptions $Bi \ll 1$, $L = O(1)$. The formal limit $L \to 0$ taken in the framework of the previous theory, corresponds to the case $Bi \ll L \ll 1$, and it does not include the important cases $Bi = O(L)$ and $Bi \gg L$. Also, only the longwave type of instability was studied.

In the present paper, we consider the Rayleigh-Marangoni instability of a binary fluid layer or a layer of nano-fluid in the case where both Bi and L are small. In Sec. 2, we formulate a mathematical model applicable for both binary solutions and nanofluids. Sec. 3 contains the main results of the linear stability analysis for both monotonic and oscillatory instability modes. Sec. 4 contains the discussion of results and the conclusions.

2 Formulation of the Model

As stated in the introduction, we consider both binary solutions and nano-fluids. The formulation of the model that describes the Rayleigh-Marangoni convection in

a binary liquid is well known, and we refer the reader to the books [Colinet, Legros, and Velarde (2001); Nepomnyashchy, Velarde, and Colinet (2002)]. In the present section, we discuss in more detail the case of nanofluids.

In order to develop a realistic two-component model for transport phenomena in nanofluids, it is important to understand the mechanisms by which the nanoparticles can develop a slip velocity with respect to the carrier fluid. According to the estimates in [Buongiorno (2006)], Brownian diffusion and thermophoresis are important as slip mechanisms, while gravity settling is negligible. Thus, the diffusion mass flux for the nanoparticles can be written as the sum of two components: the term proportional to the concentration gradient $\vec{j}_{p,B}$, representing Brownian diffusion, whereas the term proportional to the temperature gradient $\vec{j}_{p,T}$, which is identical to that corresponding to the Soret effect in a binary solution, represents thermophoresis

$$\vec{j}_p = \vec{j}_{p,B} + \vec{j}_{p,T} = -\rho_p D_B \nabla c - \rho_p D_T \frac{\nabla \vartheta}{\vartheta}. \tag{1}$$

Here $D_B = \dfrac{k_B\,\vartheta}{3\,\pi\,\mu\,d_p}$ is Brownian diffusion coefficient ranging from 4×10^{-10} to $4\times10^{-12}\ m^2/s$, k_B is Boltzmann's constant, ϑ is temperature, μ is dynamic viscosity of the fluid ($\mu \sim 1\ mPa\ s$), d_p is nanoparticle diameter $d_p < 100\ nm$, ρ_p is the mass density of the nanoparticles ($\rho_p \sim 4\ g/cm^3$), c is nanoparticle volumetric fraction, $D_T = \delta\,\dfrac{\mu}{\rho}\,c$ is "thermal diffusion coefficient", $\delta = \delta(k_{th}, k_{th}^{(p)})$ is the function of both thermal conductivity of the fluid k_{th} and that of the particle material $k_{th}^{(p)}$. For instance, for alumina nanoparticles in water $\delta \sim 0.006$.

We consider a fluid layer under terrestrial gravity conditions subjected to a transverse temperature gradient. A concentration gradient is induced due to the Soret effect. The layer is exposed to the ambient gas phase at its nondeformable free surface.

In the framework of our theory we consider two convection mechanisms. First, surface tension is assumed to depend on both temperature and solute concentration, hence both Marangoni, thermo- and soluto -capillary effects are taken into account:

$$\sigma(\vartheta, c) = \sigma_0 - \sigma_t(\vartheta - \vartheta_0) + \sigma_c(c - c_0), \tag{2}$$

where $\sigma_0 = \sigma(\vartheta_0, c_0)$ $\sigma_t = -\partial\sigma/\partial\vartheta$, $\sigma_c = \partial\sigma/\partial c$.

In the case of binary solution, the approximation (2) is standard. In the case of a nanofluid, the very idea of using a *thermodynamic equilibrium* relation between the surface tension σ and the concentration of nanoparticles c needs some comments. A significant influence of the nanoparticle concentration on the surface tension was

observed in experiments [Okubo (1995); Xue, Fan, Hu, Hong, and Cen (2006); Dong and Johnson (2003b); Dong and Johnson (2003a); Ravera, Ferrari, Liggieri, Loglio, Santini, and Zanobini (2008)]. However, there is a strong evidence that under conditions of a real experiment, a true thermodynamic equilibrium between the bulk and interface is never achieved [Steinchen (2008)]. We leave the analysis of the physical roots of the surface tension dependence on the particle concentration, as well as the incorporation of more delicate non-equilibrium and nonlinear effects, such as ordering and aggregation of particles at the interface for a future research. In the present paper, we will use assumption (2) which seems to be sufficient for the development of a linear stability theory.

The liquid density ρ is assumed to depend on both the temperature ϑ and solute concentration c,

$$\rho = \bar{\rho}[1 - \widetilde{\beta}(\vartheta - \bar{\vartheta}) - \widetilde{\gamma}(c - \bar{c})], \tag{3}$$

where $\bar{\rho}, \bar{\vartheta}, \bar{c}$ are, respectively, reference values of density, temperature and solute concentration, $\widetilde{\beta} = -\frac{1}{\bar{\rho}}\left(\frac{\partial \rho}{\partial \vartheta}\right)_p$, $\widetilde{\gamma} = -\frac{1}{\bar{\rho}}\left(\frac{\partial \rho}{\partial c}\right)_p$. Thus, the effect of buoyancy is included in the analysis. Recall that in the layer, where a combination of Rayleigh and Marangoni convection takes place, deformation of the free surface is irrelevant.

The set of conservation equations for nanofluids consists of the continuity equation (4), the momentum equation (5) in the Oberbeck-Boussinesq approximation, so that gravity results in the buoyancy force produced by temperature and concentration stratification, the nanofluid energy equation (6) and the nanoparticle continuity equation (7) [Buongiorno (2006)]:

$$\nabla \cdot \vec{v} = 0, \tag{4}$$

$$\vec{v}_t + (\vec{v} \cdot \nabla)\vec{v} = -\rho_0^{-1} \nabla p + \nu \nabla^2 \vec{v} + \widetilde{\beta}(\vartheta - \overline{\vartheta})\vec{e}_z + \widetilde{\gamma}(c - \overline{c})\vec{e}_z, \tag{5}$$

$$\vartheta_t + \vec{v} \cdot \nabla \vartheta = \kappa \nabla^2 \vartheta + \frac{\rho_p \eta_p}{\rho \eta}\left\{ D_B \nabla c \cdot \nabla \vartheta + D_T \frac{\nabla \vartheta \cdot \nabla \vartheta}{\vartheta} \right\}, \tag{6}$$

$$c_t + \vec{v} \cdot \nabla c = \nabla \left\{ D_B \nabla c + D_T \frac{\nabla \vartheta}{\vartheta} \right\}. \tag{7}$$

Here, $\nabla = \left\{ \frac{\partial}{\partial x}, \frac{\partial}{\partial y} \right\}$, ν is kinematic viscosity, κ is thermal diffusivity, ρ is fluid density ($\rho \sim 1\, g/cm^3$), η is nanofluid specific heat, η_p is nanoparticle specific heat, and $\overline{\vartheta}, \overline{c}$ are constant average values of the temperature and concentration, respectively. The third equation (6) states that heat can be transported in nanofluids by convection (second term in the left-hand side), conduction (first term in the

right-hand side) and also by nanoparticle diffusion (second and third terms in the right-hand side). It should be noted that two last terms in the right-hand side in the nanofluid energy equation (6) account for the additional contribution associated with the nanoparticle motion relative to the carrier fluid. The last equation (7) states that nanoparticles can move homogeneously with the fluid (second term in the left-hand side), but they also possess a slip velocity relative to the fluid due to Brownian diffusion and thermophoresis.

To estimate the relative importance of the various transport mechanisms in nanofluids, it is useful to make the conservation equations non-dimensional. For this purpose we use the following standard scaling

$$
\begin{aligned}
&t \to \frac{h_0^2}{\nu} t,\ (x,z) \to h_0 (x,z),\ (u,w) \to \frac{\kappa}{h_0} (u,w), \\
&\vartheta \to \vartheta_\infty + a h_0 T,\ \Delta\vartheta \equiv a h_0 = \vartheta_0 - \vartheta_\infty, \\
&c \to \frac{\sigma_t}{\sigma_c} a h_0 C,\ p \to \frac{\mu\kappa}{h_0^2} p.
\end{aligned}
\tag{8}
$$

The system (4-7) takes form

$$
\begin{aligned}
&\nabla \cdot \vec{v} = 0, \\
&\vec{v}_t + P^{-1} (\vec{v} \cdot \nabla) \vec{v} = -\nabla p + \nabla^2 \vec{v} + r_{th}\, (T - \overline{T}) \cdot \vec{e}_z + r_c\, (C - \overline{C}) \cdot \vec{e}_z, \\
&P T_t + \vec{v} \cdot \nabla T = \nabla^2 T + K_C \nabla C \cdot \nabla T + K_T \nabla T \cdot \nabla T, \\
&P L^{-1} C_t + L^{-1} \vec{v} \cdot \nabla C = \nabla^2 C + \chi \nabla^2 T,
\end{aligned}
\tag{9}
$$

where the last term of the fourth equation in (9) stands for the Soret effect taken into account. Also, we assume $\dfrac{\delta\vartheta}{\vartheta_\infty} \ll 1$ applying linearization around a certain reference temperature in the equations (6) and (7).

Order-of-magnitude estimations of the contribution of each term in the non-dimensional nanofluid energy equation show that heat transfer associated with nanoparticle dispersion is negligible compared with heat conduction and convection:

$$
\begin{aligned}
K_C &= \frac{\rho_p \eta_p}{\rho \eta} \cdot \frac{D_B}{\kappa} \cdot \frac{\sigma_t}{\sigma_c} \cdot \Delta\vartheta \sim 10^{-5}, \\
K_T &= \frac{\rho_p \eta_p}{\rho \eta} \cdot \frac{D_T}{\kappa} \cdot \frac{\Delta\vartheta}{\vartheta_\infty} \sim 10^{-6}.
\end{aligned}
\tag{10}
$$

Therefore, the consistent model for the description of hydrodynamics and heat transfer in nanofluids is identical to the set of equations for a binary mixture with

the Soret effect:

$$\begin{aligned}
&\nabla\cdot\vec{v}=0,\\
&\vec{v}_t+P^{-1}(\vec{v}\cdot\nabla)\vec{v}=-\nabla p+\nabla^2\vec{v}+r_{th}\,(T-\overline{T})\cdot\vec{e}_z+r_c\,(C-\overline{C})\cdot\vec{e}_z,\\
&PT_t+\vec{v}\cdot\nabla T=\nabla^2 T,\\
&PL^{-1}C_t+L^{-1}\vec{v}\cdot\nabla C=\nabla^2 C+\chi\nabla^2 T.
\end{aligned}\tag{11}$$

The boundary conditions at the bottom rigid surface $z=0$ reflect the no slip condition for the velocities, and a specified heat flux and mass impermeability:

$$z=0:\ \ \vec{v}=0,\ \ T_z=-1,\ \ C_z=\chi. \tag{12}$$

At the free non-deformable liquid-gas interface, the boundary conditions are, respectively, the kinematic boundary condition, heat and mass flux balance, and the balance of tangential stresses (the temperature of the gas is chosen as the reference temperature):

$$\begin{aligned}
&z=1:\ \ \vec{v}\cdot\vec{e}_z=0,\ \ T_z+BiT=0,\ \ C_z-\chi BiT=0,\\
&\partial_z u=M_{th}(C_x-T_x).
\end{aligned}\tag{13}$$

The dimensionless parameters of the problem are given as $P=\dfrac{\nu}{\kappa}$ - Prandtl number, $L^{-1}=\dfrac{\kappa}{D_B}$ - inverse Lewis number, $Bi=\dfrac{qh_0}{k_{th}}$ - Biot number, $m_{th}=\dfrac{\sigma_t a h_0^2}{\mu\kappa}$ -thermal Marangoni number, $m_c=\dfrac{\alpha\sigma_c a h_0^2}{\mu\kappa}$- concentration Marangoni number, $\chi=\dfrac{m_c}{m_{th}}=\dfrac{\alpha\sigma_c}{\sigma_t}$ - Soret number, $\alpha=\dfrac{D_T}{D_B\,\bar{\vartheta}}$, $r_{th}=\dfrac{g\widetilde{\beta}a h_0^4}{\kappa\nu}$ - thermal Rayleigh number, $r_c=\dfrac{g\widetilde{\gamma}\sigma_t a h_0^4}{\sigma_c\kappa\nu}$ - concentration Rayleigh number, $\tilde{\varphi}=\dfrac{r_c}{r_{th}}=\dfrac{\sigma_t\widetilde{\gamma}}{\sigma_c\widetilde{\beta}}$ - buoyancy separation number, $\Sigma=\dfrac{\sigma h_0}{\mu\kappa}$ - inverse capillary number.

3 Linear Stability Theory

We carry out linear stability analysis of the base state given by the following expressions:

$$\vec{v}_0=0,\ \ T_0=-z+\frac{1+Bi}{Bi},\ \ C_0=\chi z. \tag{14}$$

The expression for the base state pressure p_0 is omitted here because it is not important in the current analysis.

We introduce a stream function ψ via $u = \psi_z,\ \ w = -\psi_x$ and use it in the forthcoming derivations. A two-dimensional linear problem for the case of a non-deformable interface is solved using normal modes for perturbation functions

$$(p, T, C, \psi) = (\widetilde{p}(z), \widetilde{T}(z), \widetilde{C}(z), \widetilde{\psi}(z)) e^{ikx+\omega t}, \tag{15}$$

where k and ω are wave number and growth rate of the disturbance, respectively.

Finally, we obtain the following linear set of equations for perturbation functions:

$$\begin{aligned}
&\omega(\widetilde{\psi}'' - k^2\widetilde{\psi}) = \widetilde{\psi}'''' - 2k^2\widetilde{\psi}'' + k^4\widetilde{\psi} - ik\, r_{th}\,(\widetilde{T} + \widetilde{\varphi}\widetilde{C}),\\
&\omega P\widetilde{T} + ik\widetilde{\psi} = -k^2\widetilde{T} + \widetilde{T}'',\\
&\omega PL^{-1}\widetilde{C} - ikL^{-1}\chi\widetilde{\psi} = -k^2\widetilde{C} + \widetilde{C}'' + \chi(-k^2\widetilde{T} + \widetilde{T}'').
\end{aligned} \tag{16}$$

The boundary conditions are:

at $z = 0$:

$$\widetilde{\psi} = \widetilde{\psi}' = 0,\ \ \widetilde{T}' = \widetilde{C}' = 0, \tag{17}$$

at $z = 1$:

$$\begin{aligned}
&\widetilde{\psi} = \widetilde{\psi}' = 0,\ \ \widetilde{T}_z + Bi\widetilde{T} = 0,\ \ \widetilde{C}_z - \chi Bi\widetilde{T} = 0,\\
&\widetilde{\psi}'' = ikm_{th}(\widetilde{C} - \widetilde{T}),
\end{aligned} \tag{18}$$

where primes denote derivatives with respect to z.

We study the case of the combined long-wave Marangoni-Rayleigh convection of the system with poorly conducting boundaries in the limit of asymptotically small Lewis numbers. The behavior of the critical Marangoni and Rayleigh numbers is determined by the relationships between various small parameters of the problem, such as Biot number Bi, Lewis number L and the wave number k.

We apply a new approach in which L is considered as a basic small parameter, while the smallness of k and Bi with respect to L can be different. This approach, which is especially important in the case of nanofluids, reveals an essential difference in the scaling of the monotonic and oscillatory instability thresholds and the shape of the eigenfunctions. Thus, consideration of the nanofluids, even in the framework of the binary-fluid model, leads to solution of new non-trivial mathematical problems. In order to obtain the full neutral curve we consider several distinguished limits.

3.1 Monotonic instability mode

3.1.1 Long-wave combined Marangoni and Rayleigh convection.

We first consider the long-wave monotonic instability threshold $\omega = 0$ in the case when $Bi \sim L \sim k^2$. We use the following expansions for the perturbation functions, and parameters of the problem

$$\begin{aligned} &k = \varepsilon K,\ \widetilde{\psi} = \varepsilon(\Psi_0 + \varepsilon^2 \Psi_2 ...), \\ &(\widetilde{T}, \widetilde{C}) = (T_0, C_0) + \varepsilon^2 (T_2, C_2) + ... \\ &(m_{th}, r_{th}) = (m_0, r_0) + \varepsilon^2 (m_2, r_2) + ... \end{aligned} \tag{19}$$

Substituting the above expansion into the system (16)-(18) in the leading order of approximation with respect to small ε yields

$$\begin{aligned} &\Psi_{0,zzzz} - iK r_0 (T_0 + \widetilde{\varphi} C_0) = 0, \\ &T_{0,zz} = 0, \\ &C_{0,zz} + \chi T_{0,zz} = -iK\chi l^{-1} \Psi_0, \end{aligned} \tag{20}$$

at $z = 0$:

$$\Psi_0 = \Psi_{0,z} = T_{0,z} = C_{0,z} = 0, \tag{21}$$

at $z = 1$:

$$\begin{aligned} &\Psi_0 = T_{0,z} = C_{0,z} = 0, \\ &\Psi_{0,zz} = iK m_0 (C_0 - T_0). \end{aligned} \tag{22}$$

Solving the set of equations (20)-(22) results in

$$
\begin{aligned}
m_0 = &\Big\{-2\left(\left(3i-\sqrt{3}\right)e^{\gamma}+2\sqrt{3}e^{3\gamma}-\left(3i+\sqrt{3}\right)e^{i\sqrt{3}\gamma}+\right.\\
&4\left(-3i+\sqrt{3}\right)e^{\frac{\left(3+i\sqrt{3}\right)\gamma}{2}}+4\left(3i+\sqrt{3}\right)e^{\left(3+i\sqrt{3}\right)\gamma}-\left(3i+\sqrt{3}\right)e^{\left(4+i\sqrt{3}\right)\gamma}-\\
&8\sqrt{3}e^{\frac{\left(5+i\sqrt{3}\right)\gamma}{2}}-\left(-3i+\sqrt{3}\right)e^{\left(3+(2i)\sqrt{3}\right)\gamma}+4\left(-3i+\sqrt{3}\right)e^{\frac{\left(5+(3i)\sqrt{3}\right)\gamma}{2}}+\\
&\left.4\left(3i+\sqrt{3}\right)e^{\gamma+i\sqrt{3}\gamma}-8\sqrt{3}e^{\frac{3\left(\gamma+i\sqrt{3}\gamma\right)}{2}}+2\sqrt{3}e^{\gamma+(2i)\sqrt{3}\gamma}\right)l\gamma^4\Big\}/\\
&\left\{\left(3i+\sqrt{3}\right)K^2\chi\left(e^{\gamma}+e^{3\gamma}+e^{i\sqrt{3}\gamma}+18e^{\left(2+i\sqrt{3}\right)\gamma}-4e^{\frac{\left(3+i\sqrt{3}\right)\gamma}{2}}-4e^{\left(3+i\sqrt{3}\right)\gamma}+\right.\right.\\
&e^{\left(4+i\sqrt{3}\right)\gamma}-4e^{\frac{\left(5+i\sqrt{3}\right)\gamma}{2}}+e^{\left(3+(2i)\sqrt{3}\right)\gamma}-\\
&\left.\left.4e^{\frac{\left(5+(3i)\sqrt{3}\right)\gamma}{2}}-4e^{\gamma+i\sqrt{3}\gamma}-4e^{\frac{3\left(\gamma+i\sqrt{3}\gamma\right)}{2}}+e^{\gamma+(2i)\sqrt{3}\gamma}\right)\right\},
\end{aligned}
\tag{23}
$$

where $\gamma = \dfrac{K^{\frac{1}{3}}\tilde{\varphi}^{\frac{1}{6}}\chi^{\frac{1}{6}}r_0^{\frac{1}{6}}}{l^{\frac{1}{6}}}$. In the limit of small K we obtain

$$
m_0 = \frac{3\tilde{\varphi}r_0}{20}. \tag{24}
$$

On the other hand, expanding the expression (3.35) from [20] in the limit of a small Lewis number L, yields

$$
m_0 = \frac{3\tilde{\varphi}r_0}{20} + \underbrace{\frac{-3L\left(-320+\left(1+\tilde{\varphi}\right)r_0\right)}{20\chi}}_{O(L)} + \ldots \tag{25}
$$

Thus, in the limit of small K, the critical threshold $m_0(r_0)$ retains its sign and is slightly curved. This result suggests that the region $m, r = O(L)$ has to be investigated in more detail.

For this purpose, we use a modified scaling

$$
\begin{aligned}
&t \to \frac{h_0^2}{D}t,\ (x,z) \to h_0(x,z),\ (u,w) \to \frac{D}{h_0}(u,w),\\
&\vartheta \to \vartheta_\infty + ah_0T,\ ah_0 = \Delta\vartheta,\ c \to \alpha ah_0C,\ p \to \frac{\mu D}{h_0^2}p,
\end{aligned}
\tag{26}
$$

where $D = D_B$. Applying scaling (26) to our original system (4)-(7) leads to the modified system

$$\begin{aligned}
&\nabla \cdot \vec{v} = 0, \\
&P^{-1} L[\vec{v}_t + (\vec{v}\cdot\nabla)\vec{v}] = -\nabla p + \nabla^2 \vec{v} + R_{th}\,(T-\overline{T})\cdot\vec{e}_z + R_c\,(C-\overline{C})\cdot\vec{e}_z, \\
&T_t + \vec{v}\cdot\nabla T = L^{-1}\nabla^2 T + \tilde{K}_C \nabla C\cdot\nabla T + \tilde{K}_T \nabla T\cdot\nabla T, \\
&C_t + \vec{v}\cdot\nabla C = \nabla^2 C + \nabla^2 T,
\end{aligned} \tag{27}$$

where

$$\begin{aligned}
&\tilde{K}_C = \frac{\rho_p \eta_p}{\rho\,\eta}\cdot\alpha\,\Delta\vartheta \sim 15. \\
&\tilde{K}_T = \frac{\rho_p \eta_p}{\rho\,\eta}\cdot\frac{D_T}{D}\cdot\frac{\Delta\vartheta}{\vartheta_\infty} \sim 45. \\
&\tilde{K}_C,\ \tilde{K}_T \ll L^{-1} = \frac{\kappa}{D} \sim 10^7.
\end{aligned} \tag{28}$$

Therefore, using the modified scaling (26) we prove once again that the contribution of the terms which account for the additional contribution associated with the nanoparticle motion relative to the carrier fluid in the nondimensional nanoparticle energy equation is negligible compared with heat conduction and convection. Thus, system (27) can be applied for the description of the monotonic instability in the nanofluids in the framework of a binary-fluid model with the Soret effect when the two last terms in the right-hand side in the nondimensional nanoparticle energy equation can be safely omitted. In the new representation, the boundary conditions take the following form:

$$z = 0:\ \ \vec{v} = 0,\ \ T_z = -1,\ \ C_z = 1. \tag{29}$$

$$\begin{aligned}
&z = 1:\ \ \vec{v}\cdot\vec{e}_z = 0,\ \ T_z + BiT = 0,\ \ C_z - BiT = 0, \\
&\partial_z u = M_c C_x - M_{th} T_x.
\end{aligned} \tag{30}$$

Application of the modified scaling (26) leads to the new definitions of the Marangoni number, Rayleigh number and buoyancy separation ratio: $M_{th} = \dfrac{\sigma_t a h_0^2}{\mu D}$ -thermal Marangoni number, $M_c = \dfrac{\alpha\sigma_c a h_0^2}{\mu D}$ - concentration Marangoni number, $R_{th} = \dfrac{g\widetilde{\beta} a h_0^4}{D\nu}$ - thermal Rayleigh number, $R_c = \dfrac{g\widetilde{\gamma}\alpha a h_0^4}{D\nu}$ - concentration Rayleigh number, $\dfrac{\alpha\widetilde{\gamma}}{\widetilde{\beta}}$ -

buoyancy separation number. The relation between the two kinds of scaling (8) and (26) can be presented as

$$m_{th} = M_{th} L,\ r_{th} = R_{th} L,\ \widetilde{\varphi} = \varphi/\chi. \tag{31}$$

The linear set of equations for the perturbation functions in the new scaling is

$$\begin{aligned}
&\omega P^{-1} L(\widetilde{\psi}'' - k^2\widetilde{\psi}) = \widetilde{\psi}'''' - 2k^2\widetilde{\psi}'' + k^4\widetilde{\psi} - ikR_{th}\widetilde{T} - ikR_c\widetilde{C},\\
&L[\omega\widetilde{T} + ik\widetilde{\psi}] = -k^2\widetilde{T} + \widetilde{T}'',\\
&\omega\widetilde{C} - ik\widetilde{\psi} = -k^2\widetilde{C} + \widetilde{C}'' - k^2\widetilde{T} + \widetilde{T}''.
\end{aligned} \tag{32}$$

The linearized boundary conditions are:
at $z = 0$:

$$\widetilde{\psi} = \widetilde{\psi}' = 0,\ \ \widetilde{T}' = \widetilde{C}' = 0, \tag{33}$$

at $z = 1$:

$$\widetilde{\psi} = 0,\ \ \widetilde{T}' + Bi\widetilde{T} = 0,\ \ \widetilde{C}' - Bi\widetilde{T} = 0,\ \ \widetilde{\psi}'' = ik(M_c\widetilde{C} - M_{th}\widetilde{T}). \tag{34}$$

Substituting standard expansions (19) along with

$$(M_{th}, R_{th}) = (M_0, R_0) + \varepsilon^2(M_2, R_2) + ... \tag{35}$$

into the set (32)-(34) for both limits $k^2 \sim L$ and $k^4 \sim L$ yields in the leading order of approximation the expression for the monotonic instability threshold

$$1 - \frac{\chi M_0}{48} + \frac{\varphi R_0}{320} = 0, \tag{36}$$

that can be recast upon introduction of the Bond number $B = R_{th}/M_{th}$ in the form

$$M_0 = \frac{960}{-3B\varphi + 20\chi}. \tag{37}$$

The second-order correction in the subcase $k^4 \sim L$, i.e., $k = \varepsilon K,\ L = \varepsilon^4 l,\ Bi = \varepsilon^4\beta$ is given by

$$M_2 = \frac{-640K^2\left(261B^2\varphi^2 - 3608B\varphi\chi + 9240\chi^2\right)}{231(3B\varphi - 20\chi)^3}. \tag{38}$$

Therefore, the long-wave monotonic instability with $k_c = 0$ sets in when $B\varphi/\chi < 3.3945$ and when $B\varphi/\chi > 10.4292$ (Fig. 1).

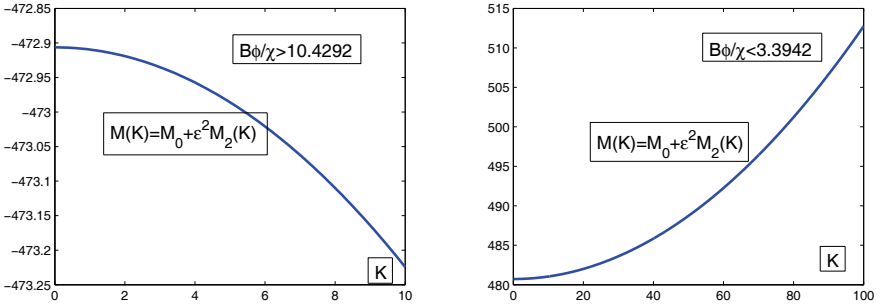

Figure 1: Long-wave monotonic neutral curves in the limit $k = \varepsilon K$, $L = \varepsilon^4 l$, $Bi = \varepsilon^4 \beta$.

In the next subcase $k = \varepsilon K$, $L = \varepsilon^2 l$, $Bi = \varepsilon^2 \beta$, the second-order correction to the monotonic instability threshold can be written as

$$M_2 = A K^2 \left[1 - \frac{F}{K^2 + \beta} \right], \tag{39}$$

where

$$A = \frac{M_2|_{K^4 \sim L}}{K^2}, \; F = \frac{693 l (3B\varphi - 20\chi)(3B(\varphi - 1) - 20(1 + \chi))}{522 B^2 \varphi^2 - 7216 B \varphi \chi + 18480 \chi^2}. \tag{40}$$

Our analysis shows that in this limit in the parameter regions $B\varphi/\chi < 3.3945$ and $B\varphi/\chi > 10.4292$, the monotonic neutral curve has a minimum of the absolute value in the long-wave region either at $K_c^{(\beta)} = 0$ for $F^{(\beta)} \leq 1$ (Fig.2a), or at finite $K_c^{(\beta)} = \sqrt{\sqrt{F^{(\beta)}} - 1}$ for $F^{(\beta)} > 1$ (Fig.2b), where $K_c^{(\beta)} = K/\sqrt{\beta}$, $F^{(\beta)} = F/\sqrt{\beta}$. It should be noted that the previous limit is a particular case of the latter when K tends to infinity.

Next, we consider the limit of $Bi \sim L^2$ and $L \sim k$: $k = \delta K$, $L = \delta l$, $Bi = \delta^2 \beta$. In this case, the higher-order correction can be obtained from the previous case when $k = O(\sqrt{L})$ in the limit of a small K

$$\lim_{K \to 0} M_2|_{k \simeq \sqrt{L}} = M_1 = \frac{960 l K^2 [3B(\varphi - 1) - 20(1 + \chi)]}{(K^2 + \beta)(3B\varphi - 20\chi)^2}. \tag{41}$$

Depending on the parameters of the problem the minimum of the full monotonic neutral curve is obtained either at $k = 0$ or it is located beyond the region $k = O(\delta)$ (Fig.3).

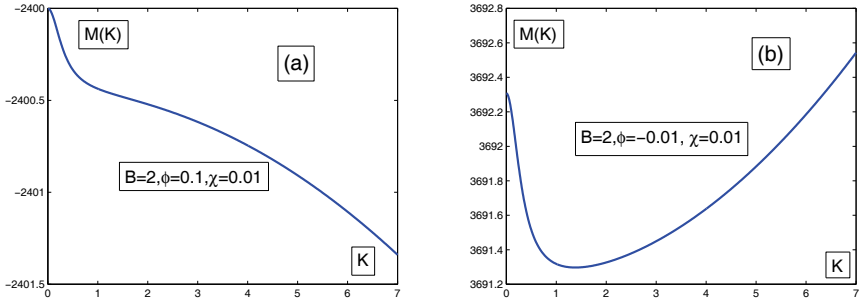

Figure 2: Typical forms of the long-wave monotonic neutral curve in the limit.

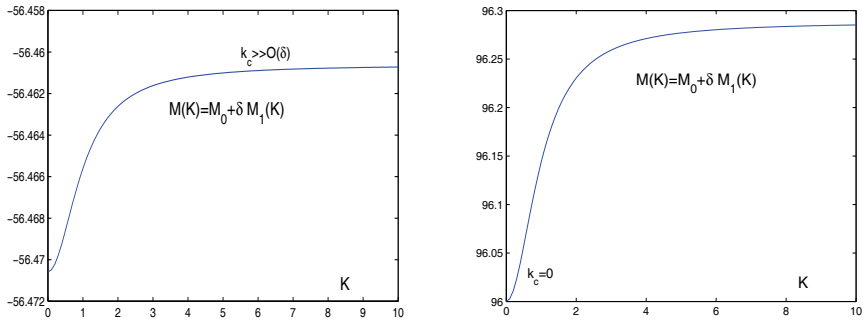

Figure 3: Examples of the monotonic neutral curves in the limit $Bi \sim L^2$ and $L \sim k$: $k = \delta K$, $L = \delta l$, $Bi = \delta^2 \beta$. Depending on the problem parameters the minimum of the full monotonic neutral curve is attained at $k = 0$ (right panel), when $M_0 > 0, M_1 > 0$ ((36), (41)) or the minimum is located beyond the region $k = O(\delta)$ (left panel), when $M_0 < 0, M_1 > 0$ ((36), (41)).

It should be noted that in the limit $k = \varepsilon K$, $L = \varepsilon^2 l$, $Bi = \varepsilon^4 \beta$, using scaling (8) for the monotonic instability problem we can examine the asymptotic behavior of the monotonic neutral curve for $K \gg 1$. Our analysis reveals that for $\widetilde{\varphi}\chi r_0 > 0$, the minimum of the neutral curve is located beyond the region $k = O(\varepsilon)$

$$m_0 = \frac{2l\delta^4}{K^{2/3}\chi}, \tag{42}$$

where $\delta = |\widetilde{\varphi}\chi r_0|^{1/6}/l^{1/6}$. Thus, in this subcase a new analysis in the short-wave domain is essential.

We complete our investigation of the monotonic instability for small Lewis numbers by a numerical investigation of the region of finite wave numbers. Our analysis shows that for both ways of heating, the neutral curves exist for all Bond numbers. When $B < 3.3945$, the minimum is attained at zero for heating from below and in the region of finite k for heating from above, see Fig.4. When $B > 10.4292$, the situation is opposite: the long-wave instability appears for heating from above and the short-wave one for heating from below, see Fig.5. In the intermediate region, for both ways of heating the minimum is attained in the region of finite wave numbers, but the sign of $M(k=0)$ changes at $B = 6.667$, as shown in Figs.6-8. In Fig. 9, the variations of the minimum value of the monotonic Marangoni number and of the corresponding critical wave number with the Bond number are presented. A numerical investigation shows that for heating from above with a decrease in the Bond number, the minimal Marangoni number tends to infinity when the Bond number approaches a certain finite value. Figure 10 presents the variation of the minimal value of the critical Rayleigh number with the Bond number ($\varphi = 0.5$), see the left panel, and that of the critical Rayleigh number versus the critical Marangoni number, see the right panel, for the case of monotonic instability in the limit $Bi \sim L^2$, $k = O(1)$.

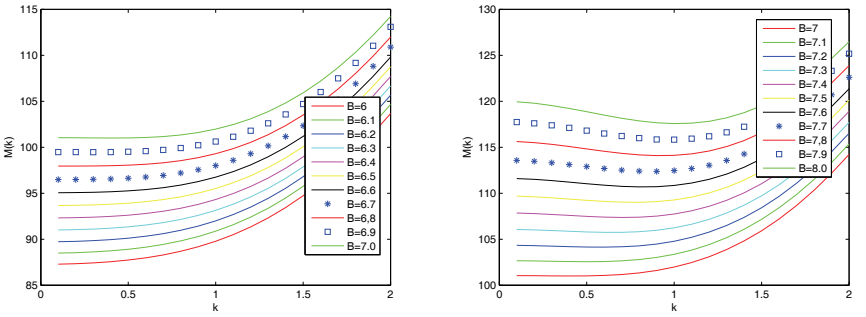

Figure 4: Examples of the monotonic neutral curves in the limit $Bi \sim L^2$, $k = O(1)$ in the region $B\varphi < 3.3945$, (for $\varphi = 0.5$). When $B\varphi < 3.3945$, the minimum is attained at zero for heating from below, whereas for heating from above it is located in the domain of finite k. When $B\varphi$ exceeds this value, the minimum of the neutral curve appears for $k \neq 0$ for heating from below.

3.1.2 Long-wave Rayleigh convection.

When the fluid layer is relatively thick, the buoyancy effect becomes dominant because the Rayleigh number is proportional to the fourth power of the layer depth,

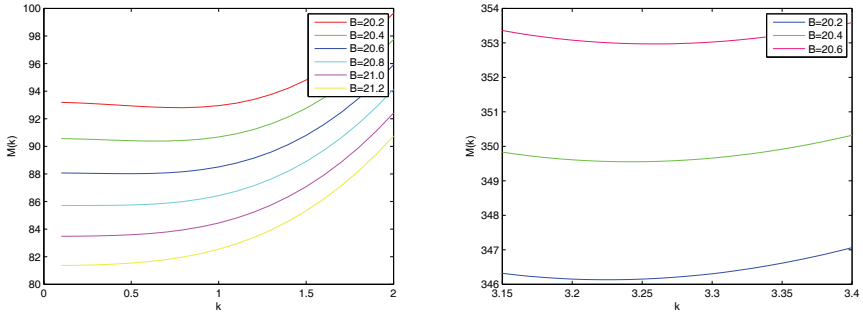

Figure 5: Examples of the monotonic neutral curves in the limit $Bi \sim L^2$, $k = O(1)$ in the domain $B\varphi > 10.4292$, (for $\varphi = 0.5$). When $B\varphi$ exceeds this value, the minimum of the neutral curve is located at $k = 0$ for heating from above. For heating from below the minimum of the neutral curve is attained in the region of finite wave numbers.

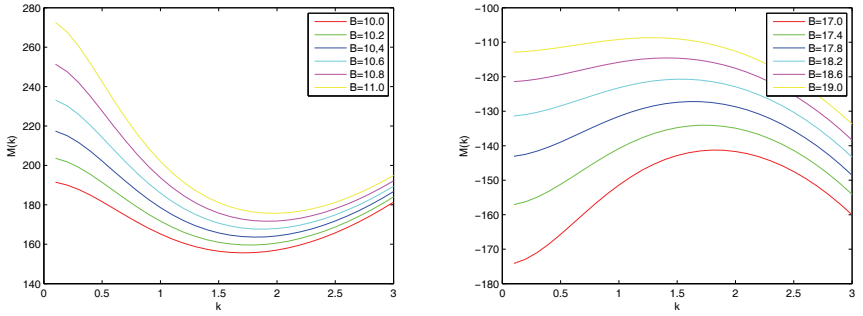

Figure 6: Examples of the monotonic neutral curves in the limit $Bi \sim L^2$, $k = O(1)$ in the domain $3.3945 < B\varphi < 10.4292$, (for $\varphi = 0.5$). When $B\varphi > 6.667$, the sign of the monotonic neutral curve changes.

$Ra \sim h^4$, whereas the Marangoni number is proportional to the squared layer depth, $Ma \sim h^2$. Assuming the limit of asymptotically small Lewis numbers $k = O(1)$, $L = O(\varepsilon^2)$, $R_0 = O(1)$, $M_0 = 0$ in the leading order of approximation with respect to the small ε we obtain the following problem for the concentration perturbation

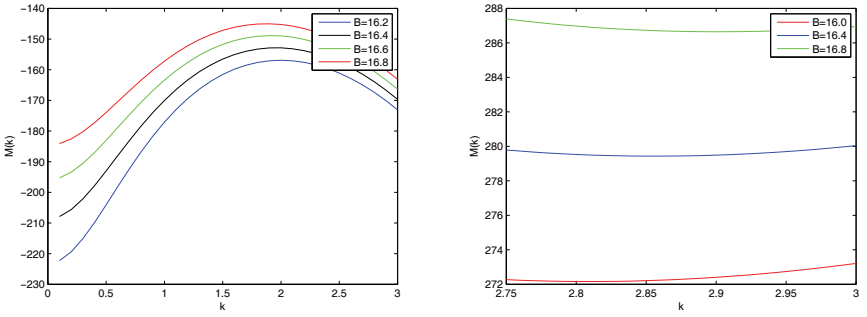

Figure 7: Examples of the monotonic neutral curves in the limit $Bi \sim L^2$, $k = O(1)$ in the domain $3.3945 < B\varphi < 10.4292$, (for $\varphi = 0.5$). For both directions of heating the neutral curves emerge with a minimum in the region of finite wave numbers.

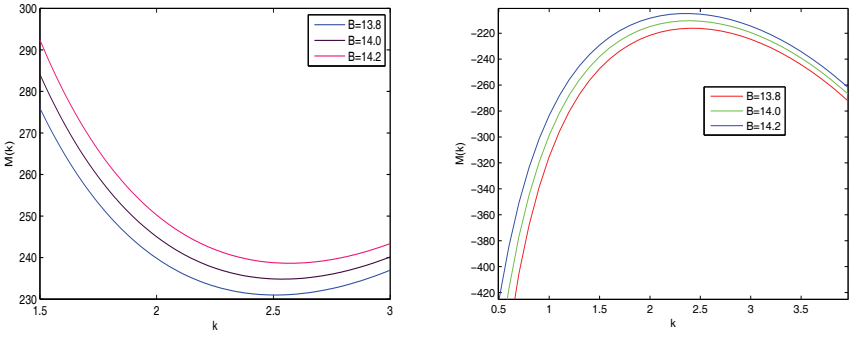

Figure 8: Examples of the monotonic neutral curves in the limit $Bi \sim L^2$, $k = O(1)$ in the domain $3.3945 < B\varphi < 10.4292$, (for $\varphi = 0.5$). For both directions of heating the neutral curves emerge with a minimum in the region of finite wave numbers.

function:

$$
\begin{aligned}
& C_0^{VI}(z) - 3k^2 C_0^{IV}(z) + 3k^4 C_0''(z) - k^2 C_0(z)(k^4 + \varphi R_0) = 0, \\
& z = 0: \; C_0' = 0, \; -k^2 C_0 + C_0'' = -k^2 C_0' + C_0''' = 0, \\
& z = 1: \; C_0' = 0, \; -k^2 C_0 + C_0'' = -k^2 C_0'' + C_0'''' = 0.
\end{aligned} \tag{43}
$$

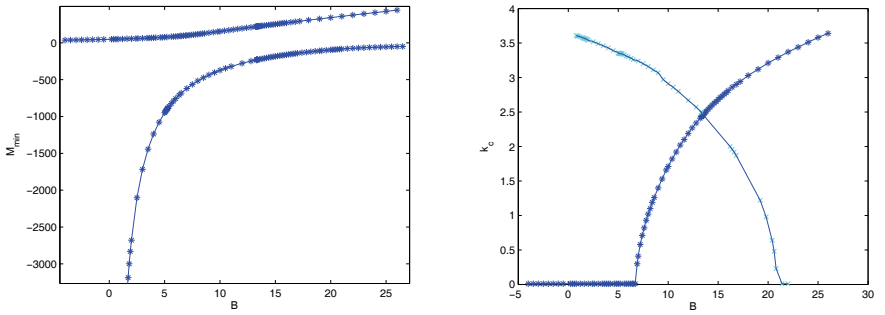

Figure 9: Variation of the minimal value of the monotonic Marangoni number (left panel) and of the corresponding critical wave number (right panel) with the Bond number ($\varphi = 0.5$) in the limit $Bi \sim L^2$, $k = O(1)$. Our analysis shows that for both ways of heating, the neutral curves exist for all Bond numbers. When $B\varphi < 3.3945$, the minimum is attained at $k = 0$ for heating from below and in the region of finite k for heating from above. When $B\varphi > 10.4292$, the situation is opposite.

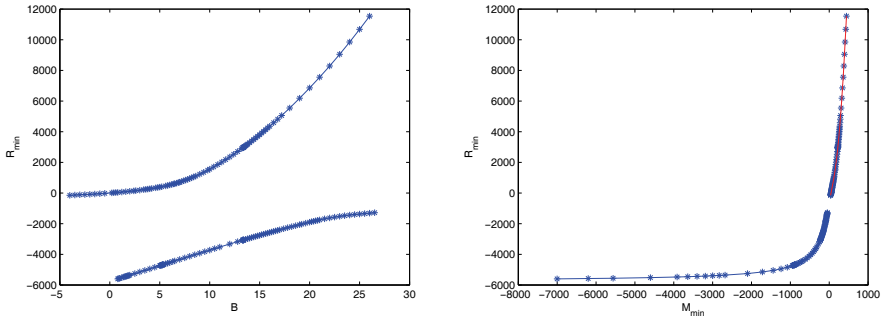

Figure 10: Variation of the minimal value of the monotonic Rayleigh number with the Bond number ($\varphi = 0.5$) (left panel) and of the critical Rayleigh number with the critical Marangoni number (right panel) in the case of the monotonic instability in the limit $Bi \sim L^2$, $k = O(1)$.

Assuming the long-wave limit when $k \ll 1$, we use following expansions with respect to a small k:

$$\begin{aligned} C_0(z) &= c_0(z) + k^2 c_2(z) + \ldots \\ R_0 &= r_0 + k^2 r_2 + \ldots . \end{aligned} \tag{44}$$

Solving (43) with (44) we obtain

$$r_0 = -\frac{320}{\varphi},\ r_2 = -\frac{18560}{693\,\varphi}. \tag{45}$$

Thus, in the case of a pure buoyancy convection in the limit of asymptotically small Lewis numbers, the minimum of the neutral curve is always located at $k = 0$. We conclude that the standard assumption that in the case of poorly conducting boundaries (for a small Biot number), the longwave convection sets in, is correct for both pure Rayleigh convection ($B \to \infty$) and pure Marangoni convection ($B = 0$). However, it is violated for the combined convection in the interval $3.3945 < B < 10.4292$. In the latter, short-wave disturbances can significantly reduce the stability region.

3.2 Oscillatory instability mode

We proceed with investigation of the onset of long-wave oscillatory instability in the framework of linear stability theory applying standard scaling (8) and assumimg the limit $k = \varepsilon K$, $L = \varepsilon^2 l$, $Bi = \varepsilon^4 \beta$ with $\varepsilon \ll 1$.

We use the following expansion for perturbation functions (stream function, temperature and concentration)

$$\widetilde{\psi} = \varepsilon\widetilde{\Psi} = \varepsilon(\Psi_0 + \varepsilon^2\Psi_2 + ...),\ \ \widetilde{T},\widetilde{C} = (T_0, C_0) + \varepsilon^2(T_2, C_2) + \ldots, \tag{46}$$

and for the growth rate, the thermal Rayleigh and Marangoni numbers, respectively,

$$\omega = \varepsilon^2(\omega_0 + \varepsilon^2\omega_2 + ...),\ \ r_{th}, m_{th} = (r_0, m_0) + \varepsilon^2(r_2, m_2) + \ldots. \tag{47}$$

Substituting these expansions into the linearized system for the amplitudes of perturbation functions with boundary conditions (16)-(18) yields in the leading order of approximation

$$\begin{aligned} &\Psi_{0,zzzz} - iK\,r_0(T_0 + \widetilde{\varphi}\,C_0) = 0,\\ &T_{0,zz} = 0,\\ &C_{0,zz} + \chi\,T_{0,zz} = \omega_0\,P\,l^{-1}C_0 - iK\,\chi\,l^{-1}\Psi_0, \end{aligned} \tag{48}$$

at $z = 0$:

$$\Psi_0 = \Psi_{0,z} = T_{0,z} = C_{0,z} = 0, \tag{49}$$

at $z = 1$:

$$\begin{aligned} &\Psi_0 = T_{0,z} = C_{0,z} = 0,\\ &\Psi_{0,zz} = iK\,m_0(C_0 - T_0). \end{aligned} \tag{50}$$

The solvability condition in the next order of approximation ε^2 reads

$$\omega_0 P T_0 + iK \int_0^1 \Psi_0 dz = -K^2 T_0. \tag{51}$$

Introducing $\Psi_0 = iK\Phi_0$ and $\omega_0 = K^2\Lambda_0$, we study the limit of small wave numbers K and look for the solution in the form of series with respect to K^2

$$\begin{aligned} &\Phi_0 = \Phi_0^{(0)} + K^2\Phi_0^{(2)} + \ldots, \;\; (T_0, C_0) = (T_0^{(0)}, C_0^{(0)}) + K^2(T_0^{(2)}, C_0^{(2)}) + \ldots, \\ &m_0 = m_0^{(0)} + K^2 m_0^{(2)} + \ldots, \;\; \Lambda_0 = \Lambda_0^{(0)} + K^2\Lambda_0^{(2)} + \ldots. \end{aligned} \tag{52}$$

Looking for the onset of the oscillatory instability threshold we set the real part of Λ_0 to zero, i.e., $\Lambda_0 = i\Omega_0$, where

$$\Omega_0 = \Omega_0^{(0)} + K^2\Omega_0^{(2)} + \ldots. \tag{53}$$

Assuming that $T_0 = 1$, i.e., $T_0^{(0)} = 1$, $T_0^{(2)} = 0$, and using the solvability condition at zero order of approximation with respect to small K in the form

$$P\Lambda_0^{(0)} - \int_0^1 \Phi_0^{(0)}(z) dz = -1, \tag{54}$$

we obtain

$$\begin{aligned} &960P\Lambda_0^{(0)}\left(1 + P\Lambda_0^{(0)}\right) - 20m_0\left(\chi + P(1+\chi)\Lambda_0^{(0)}\right) + \\ &3r_0\left(\widetilde{\varphi}\chi + P\left(\widetilde{\varphi}\chi - 1\right)\Lambda_0^{(0)}\right) = 0. \end{aligned} \tag{55}$$

It is possible to separate between the real and imaginary parts of the expression (55) and to obtain

$$\Omega_0^{(0)^2} = -\frac{\chi\,(20m_0 - 3\,\widetilde{\varphi}\,r_0)\,(20\,(1+\chi)\,m_0 - 3\,(-1+\widetilde{\varphi}\,\chi)\,r_0)}{921600\,P^2}, \tag{56}$$

and

$$1 - \frac{m_0}{48}(1+\chi) + \frac{r_0}{320}(\widetilde{\varphi}\chi - 1) = 0, \tag{57}$$

where $\Lambda_0^{(0)} = i\Omega_0^{(0)}$, and $\widetilde{\varphi}$, χ are separation numbers.
Substituting (57) into (56) we finally obtain

$$\Omega_0^{(0)^2} = \frac{\chi\,(-320 + (1+\widetilde{\varphi})\,r_0)}{320\,P^2\,(1+\chi)}. \tag{58}$$

Thus, oscillatory instability sets in when $-1 < \chi < 0$ for $|r_0| < 320/|1+\widetilde{\varphi}|$ and when $\chi < -1, \chi > 0$ for $|r_0| > 320/|1+\widetilde{\varphi}|$.

Using a second-order correction to the oscillatory instability threshold we determine the parameter domains for the Soret number, separation ratio and Rayleigh number, where destabilization takes place with the growth of the wave number K. Typical variations of the monotonic and oscillatory instability boundaries are examined in all distinguished parameter limits.

Using the solvability condition at fourth order with respect to small K in the form

$$\int_0^1 \left[P l^{-1} \left\{ \Lambda_0^{(0)} C_0^{(2)} + \Lambda_0^{(2)} C_0^{(0)} \right\} + \chi\, l^{-1}\, \Phi_0^{(2)} \right] dz = 0, \tag{59}$$

we obtain

$$\Omega_0^{(2)} = -\frac{(1+\widetilde{\varphi})\,\chi^2 r_0\,(-3520+(11+\widetilde{\varphi}\,(16+5\,\chi))\,r_0)}{283852800\,l\,P^2\,(1+\chi)^2\,\Omega_0}, \tag{60}$$

$$\Omega_0^2 = {\Omega_0^{(0)}}^2 + 2K^2\Omega_0^{(0)}\Omega_0^{(2)} + O(K^4),$$

and therefore,

$$\Omega_0^2 = \frac{\chi\,(-320+(1+\widetilde{\varphi})\,r_0)}{320\,P^2\,(1+\chi)} - \frac{K^2\,(1+\widetilde{\varphi})\,\chi^2 r_0\,(-3520+(11+\varphi\,(16+5\,\chi))\,r_0)}{141926400\,l\,P^2\,(1+\chi)^2} + O(K^4), \tag{61}$$

The second-order correction to the critical Marangoni number in the oscillatory case with respect to small K reads

$$m_0^{(2)} = \frac{1}{22176000\,l\,(1+\chi)^2}\chi\,(-35481600-1760(\widetilde{\varphi}(85\,\chi-26)-111)r_0- (\widetilde{\varphi}\chi-1)(\widetilde{\varphi}(241\,\chi-23)-264)r_0^2)\,. \tag{62}$$

Rewritten in terms of the Bond number the full oscillatory neutral curve is given by

$$m_0 = m_0^{(0)} + K^2 m_0^{(2)} + O(K^4) = \frac{960}{20(1+\chi)+3B(1-\widetilde{\varphi}\chi)} \cdot$$

$$\cdot \left\{ 1 - K^2 \frac{\chi\,(165+4620\,(1+\chi)+\widetilde{\varphi}\,(-11\,(26+41\,\chi)+36\,(-1+\widetilde{\varphi}\chi)))}{6930l\,(1+\chi)\,(3-3\,\widetilde{\varphi}\,\chi+20\,(1+\chi))} \right\} +$$

$$+O(K^4). \tag{63}$$

Depending on the parameters of the problem, the minimum of the full oscillatory neutral curve (63) is attained at $K = 0$ or outside the region of the validity of the used expansions (Fig.11). It follows from the latter fact that for certain parameter values our theory is inapplicable and one must use different expansions there.

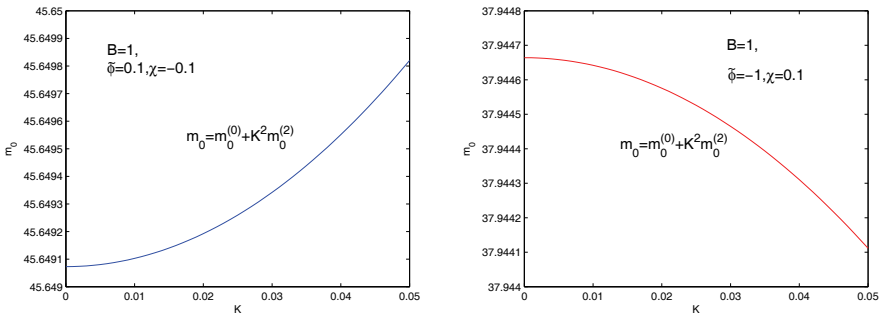

Figure 11: Full oscillatory neutral curve (63) in the limit $Bi \sim L^2 \sim k^4$. Depending on the problem parameters the minimum of this curve is attained at $K = 0$ (left panel) or outside the validity region of the expansions (right panel) used here.

3.3 Marangoni convection in very thin films

Finally, we investigate the case of pure Marangoni convection in the case of sufficiently thin films, when the buoyancy effect is neglected. We consider the monotonic instability mode in the limit $k = O(1)$, $L = O(\varepsilon^2)$, $Bi = O(\varepsilon^4)$. In the leading

order of approximation we obtain

$$\begin{aligned}
&\Psi_{0,zzzz} - 2k^2\Psi_{0,zz} + k^4\Psi_0 = 0,\\
&k^2T_0 - T_{0,zz} = 0,\\
&k^2C_0 + k^2\chi T_0 - ik\chi l^{-1}\Psi_0 - C_{0,zz} - \chi T_{0,zz} = 0,\\
&z = 0 : \Psi_0 = \Psi_{0,z} = T_{0,z} = C_{0,z} = 0,\\
&z = 1 : \Psi_0 = T_{0,z} = C_{0,z} = \Psi_{0,zz} - ikm_0(T_0 - C_0) = 0.
\end{aligned} \tag{64}$$

Solving the set (64) for the monotonic neutral curve we find

$$m_0 = \frac{16k^2l(k - \cosh(k)\sinh(k))}{2k\chi\{2 + k^2 - k\cosh(k)\} - \chi\sinh(2k)}, \tag{65}$$

which reduces in the long-wave limit $k \to 0$ to

$$m_0 = \frac{48l}{\chi} + \frac{16lk^2}{5\chi} + O(k^3). \tag{66}$$

Thus, in the case of asymptotically small Lewis numbers, the monotonic instability is always longwave.

In the more general long-wave limit of $k = q\tilde{\varepsilon}$, $Bi = \hat{\beta}\tilde{\varepsilon}^2$, $L = O(1)$, we obtain the following expressions for monotonic and oscillatory neutral curves, respectively,

$$\begin{aligned}
M_0^{mon}(q) &= \frac{48L(q^2 + \hat{\beta})}{\hat{\beta}\chi + q^2(\chi + L(1+\chi))},\\
M_0^{osc}(q) &= \frac{48(q^2(1+L) + \hat{\beta})}{q^2(1+\chi)}.
\end{aligned} \tag{67}$$

It is noteworthy that the monotonic neutral curve changes its sign through infinity at

$$q_1 = \sqrt{\frac{-\hat{\beta}\chi}{\chi + L(1+\chi)}}, \tag{68}$$

and both neutral curves merge at

$$q_2 = \sqrt{\frac{-(2+L)\hat{\beta}\chi + \hat{\beta}L\sqrt{-\chi(4+3\chi)}}{2[\chi + L(L+\chi+L\chi)]}}. \tag{69}$$

It should be noted that in the leading order of approximation, the contribution of the thermocapillary effect rapidly decreases with a decrease of the disturbance wave number, and the solutocapillary effect becomes the dominant factor triggering the instability:

$$T_0 = \frac{k^2 L}{\chi(Bi + k^2(1+L))} C_0 \Rightarrow T_0 \ll C_0, \text{ when } k^2 \ll Bi. \tag{70}$$

Typical forms of the neutral curves in the case of a pure Marangoni convection depending on the value of the Soret number are presented in Figs. 12-15.

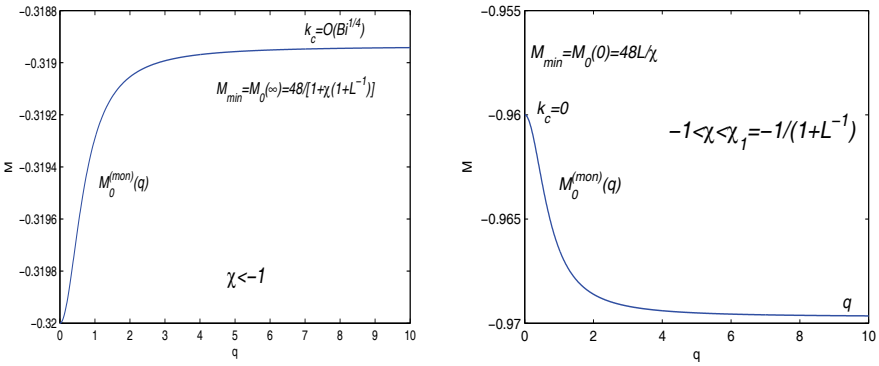

Figure 12: Examples of the neutral curves in the case of a pure Marangoni convection described by Eqs.(67). The solid curve represents the monotonic neutral curve. In the left panel, for $\chi < -1$ the minimum of the monotonic neutral curve is attained in the long-wave region $k = O(Bi^{1/4})$. In the right panel, for $-1 < \chi < \chi_1 = -1/(1+L^{-1})$ the minimum of the monotonic neutral curve is located at $k = 0$.

4 Discussion

A comparison of the obtained results with the case of a pure buoyancy convection ($m_0 = 0$) shows drastic changes of the instability criteria in the case of the combined Marangoni/Rayleigh convection. We find from Eq.(36) that the monotonic instability in the absence of the Marangoni effect can take place only for a specific way of heating, i. e., for $\varphi R_0 < 0$. At the same time, Eq.(37) shows that the instability can take place for different directions of heating depending on the relation between the buoyancy separation ratio φ and the Soret number χ. Reformulating the expression for the second-order correction to the monotonic instability threshold (39) in terms

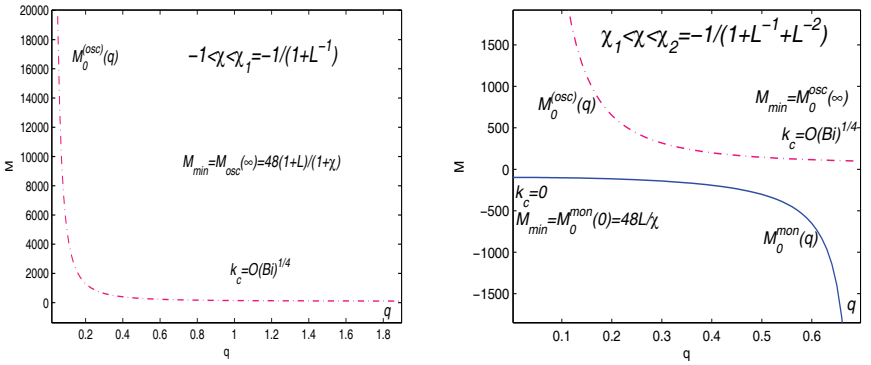

Figure 13: Examples of the neutral curves in the case of a pure Marangoni convection described by Eqs. (67). The solid and broken curves are, respectively, the monotonic and oscillatory neutral curves. In the left panel, for $-1 < \chi < \chi_1 = -1/(1+L^{-1})$ the minimum of the oscillatory neutral curve is attained in the long-wave region $k = O(Bi^{1/4})$. In the right panel, for $\chi_1 < \chi < \chi_2 = -1/(1+L^{-1}+L^{-2})$ the minimum of the monotonic neutral curve is located at $k = 0$, whereas the oscillatory neutral curve has the minimum in the long-wave domain $k = O(Bi^{1/4})$.

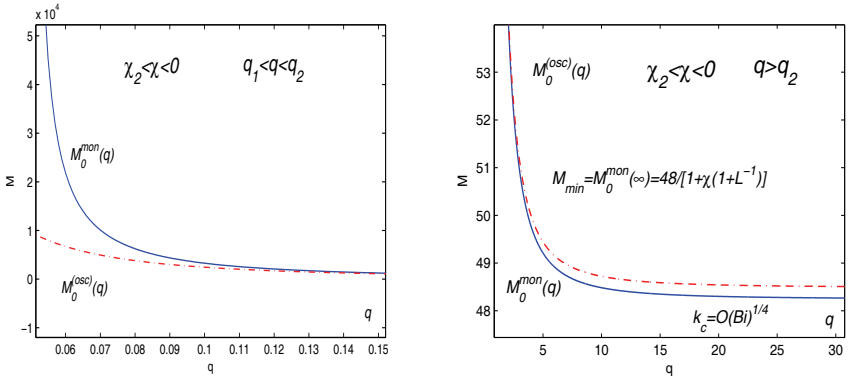

Figure 14: Examples of the neutral curves in the case of a pure Marangoni convection described by Eqs. (67). The solid and broken curves are, respectively, the monotonic and oscillatory neutral curves. In the left panel, for $\chi_2 < \chi < 0$ and $q_1 < q < q_2$ eqs. (68),(69), the oscillatory instability sets in. In the right panel, for $\chi_2 < \chi < 0$ and $q > q_2$, the monotonic instability emerges in the long-wave domain $k = O(Bi^{1/4})$.

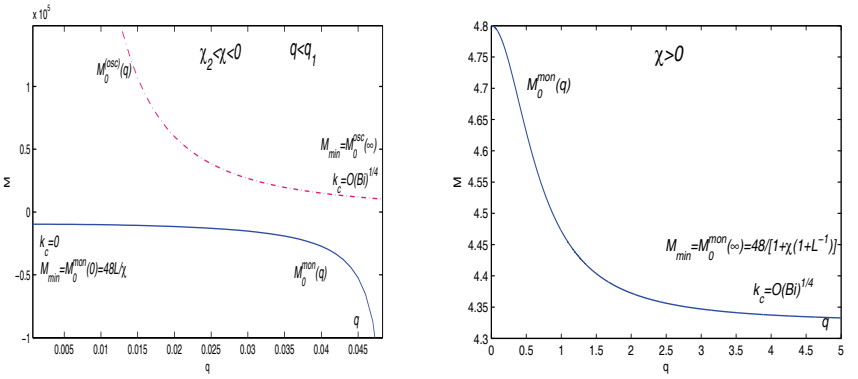

Figure 15: Examples of the neutral curves in the case of a pure Marangoni convection described by Eqs. (67). The solid and broken curves are, respectively, the monotonic and oscillatory neutral curves. on the left panel, for $\chi_2 < \chi < 0$ and $q < q_1$ eq. (68), the oscillatory instability sets in for heating from below with the wavenumber in the long-wave domain $k = O(Bi^{1/4})$, and the monotonic instability sets in for heating from above with a zero wavenumber. In the right panel, for $\chi > 0$ the monotonic neutral curve has a minimum in the long-wave domain $k = O(Bi^{1/4})$.

of R_2 and the Bond number B, and taking the limit of large Bond numbers $B \to \infty$, that corresponds to the case of a pure Rayleigh convection, we find that the minimum of the neutral curve $R_2(K)$ is located at $K_c = 0$ when $693\,l\,(\varphi-1)/(58\,\varphi) \le 1$, or this minimum is attained at finite K for $693\,l\,(\varphi-1)/(58\,\varphi) > 1$. Thus, the presence of the Marangoni effect can significantly change the stability properties of the system.

5 Conclusions

A general two-component non-homogeneous equilibrium model for transport phenomena applicable for both nanofluids and binary solutions has been formulated in this paper. In the framework of this model, we investigate a combined long-wave Marangoni and Rayleigh instability of a quiescent state of a binary (nano-) liquid layer with a non-deformable free surface and subjected to a transverse temperature gradient. Our analysis taking into account the Soret effect considers a relevant limit of asymptotically small Lewis numbers and poorly conducting boundaries. We find that in the case of small Biot numbers two important long-wave regions $k = O(Bi^{1/4})$ and $k = O(Bi^{1/2})$ exist. Typical variations of the monotonic and oscillatory instability boundaries are examined in distinct parameter limits using a new approach in which Lewis number is considered as a basic small parameter. Thus,

consideration of the nanofluids, even in the framework of a binary-fluid model, leads to the solution of new mathematical problems.

Acknowledgement: A.A.N. acknowledges the support by the Israel Ministry of Science through the Grant No. 3-5799. A. O. acknowledges the support of the Technion President Fund, Research Vice President Funds and the Fund for Promotion of Research at the Technion.

References

Buongiorno, J. (2006): Convective transport in nanofluids. *Journal of Heat Transfer*, vol. 128, pp. 240–250.

Castillo, J.; Velarde, M. (1978): Thermal diffusion and the Marangoni-Benard instability of a two-component fluid layer heated from below. *Phys. Lett. A*, vol. 66, pp. 489–491.

Colinet, P.; Legros, J.; Velarde, M. (2001): Nonlinear dynamics of surface-tension-driven instabilities. *Wiley-VCH, Berlin*.

Cross, M.; Hohenberg, P. (1993): Pattern formation outside of equilibrium. *Rev. Mod. Phys.*, vol. 65, pp. 851–1112.

Dong, L.; Johnson, D. (2003): Interfacial tension measurements of colloidal suspensions: An explanation of colloidal particle-driven interfacial flows. *Adv. Space Res.*, vol. 32(2), pp. 149–153.

Dong, L.; Johnson, D. (2003): Surface tension of charge-stabilized colloidal suspensions at the water-air interface. *Langmuir*, vol. 19, pp. 10205–10209.

Khanafer, K.; Vafai, K.; Lightstone, M. (2003): Buoyancy-driven heat transfer enhancement in a two-dimensional enclosure utilizing nanofluids. *Int. J. Heat Mass Transfer*, vol. 46, pp. 3639–3653.

Kim, J.; Jung, J.; Kang, Y. (2007): Absorption performance enhancement by nano-particles and chemical surfactants in binary nanofluids. *Int. J. Refrigeration*, vol. 30, pp. 50–57.

Kim, J.; Kang, J.; Choi, C. (2007): Soret and Dufour effects on convective instabilities in binary nanofluids for absorption application. *Int. J. Refrigeration*, vol. 30, pp. 323–328.

Kim, J.; Kang, Y.; Choi, C. (2004): Analysis of convective instability and heat transfer characteristics of nanofluids. *Phys. Fluids*, vol. 16, pp. 2395–2401.

Kim, J.; Kang, Y.; Choi, C. (2005): Effects of thermodiffusion and nanoparticles on convective instabilities in binary nanofluids. *J. Nanoscale Microscale Therm. Eng.*, vol. 10(1), pp. 29–39.

Kim, M.; Hong, J.; Choi, C. (2006): The analysis of the onset of Soret-driven convection in nanoparticles suspension. *AIChE Jornal*, vol. 52,(7), pp. 2333–2339.

Mazzoni, S.; Cerbino, R.; Brogioli, D.; Vailati, A.; Giglio, M. (2004): Transient oscillations in Soret-driven convection in a colloidal suspension. *Eur. Phys. J.*, vol. E 15, pp. 305–309.

Nepomnyashchy, A.; Velarde, M.; Colinet, P. (2002): Interfacial phenomena and convection. *Chapman & Hall/CRC*.

Nield, D. A. (1967): The thermohaline Rayleigh-Jeffreys problem. *J. Fluid Mech.*, vol. 29, pp. 545–558.

Okubo, T. (1995): Surface tension of structured colloidal suspensions of polystyrene and silica spheres at the air-water interface. *Journal of Colloid and Interfacial Science*, vol. 171, pp. 55–62.

Oron, A.; Nepomnyashchy, A. (2004): Long-wavelength thermocapillary instability with the Soret effect. *Phys. Rev. E*, vol. E 69, pp. 016313–1–016313–17.

Podolny, A.; Nepomnyashchy, A.; Oron, A. (2008): Long-wave coupled Marangoni - Rayleigh instability in a binary liquid layer in the presence of the Soret effect. *Math. Model. Nat. Phenom*, vol. 3 (1), pp. 1–26.

Ravera, F.; Ferrari, M.; Liggieri, L.; Loglio, G.; Santini, E.; Zanobini, A. (2008): Liquid-liquid interfacial properties of mixed nanoparticle-surfactant systems. *Colloids and Surfaces A: Physicochem. Eng. Aspects*, vol. 323, pp. 99–108.

Ryskin, A.; Muller, H.; Pleiner, H. (2003): Thermal convection in binary fluid mixtures with a weak concentration diffusivity, but strong solutal buoyancy forces. *Phys. Rev. E*, vol. 67, pp. 46302.

Savino, R.; Paterna, D. (2008): Thermodiffusion in nanofluids under different gravity conditions. *Phys. Fluids*, vol. 20, pp. 017101.

Shliomis, M.; Souhar, M. (2000): Self-oscillatory convection caused by the Soret effect. *Europhys. Lett.*, vol. 49 (1), pp. 55–61.

Steinchen, A. (2008): From dispersed nano-objects to solutions – a thermodynamic approach. *Colloid and Surfaces A: Physicochem. Eng. Aspects*, vol. 323, pp. 163–166.

Xuan, Y.; Li, Q. (2000): Heat transfer enhancement of nanofluids. *Int. J. Heat Fluid Flow*, vol. 21, pp. 58–64.

Xuan, Y.; Roetzel, W. (2000): Conceptions for heat transfer correlation of nanofluids. *Int. J. Heat Mass Transfer*, vol. 43, pp. 3701–3707.

Xue, H.; Fan, J.; Hu, Y.; Hong, R.; Cen, K. (2006): The interface effect of carbon nanotube suspension on the thermal performance of a two-phase closed thermosyphon. *J. Appl. Phys.*, vol. 100, pp. 104909.